JOURNAL OF APPLIED PHYSICS VOLUME 42, NUMBER 1 JANUARY 1971

Emission of Microwave Noise Radiation From InSb*

W. J. Fleming and J. E. Rowe

Electron Physics Laboratory, Department of Electrical Engineering, The University of Michigan, Ann Arbor, Michigan 48104

(Received 11 May 1970; in final form 12 August 1970)

Low-field 10-GHz noise radiation and attendant rf current oscillations are generated in 10-mm-long specimens of n-type InSb at 77°K. Using a special experimental arrangement, both the azimuthal and the polar orientation of the applied magnetic field can be varied and the spatial distribution of the radiation along the length of the InSb specimen can also be measured. Two distinct modes of low-field radiation are found in InSb specimens. One mode of radiation ($B_{||}$ mode) prevails when the magnetic field is aligned parallel to the direction of current flow and the other mode of radiation ($B_{\perp}$ mode) prevails when the magnetic field is aligned transverse to the direction of current flow. The $B_{\perp}$ mode of radiation is investigated in considerable detail and it is determined that a reproducible anisotropic radiation pattern of twofold periodicity is obtained when a transverse magnetic field is rotated in the azimuthal plane around the InSb specimen. A computer analysis using a theory which incorporates an acoustoelectric interaction, involving off-axis acoustic waves, shows good agreement with the experimental azimuthal radiation patterns of the present experiment and other related experiments. It is concluded that an acoustoelectric-type interaction is involved in both the $B_{\perp}$ and $B_{||}$ modes of low-field noise radiation.

I. INTRODUCTION

In 1964 Larrabee[1] reported on the phenomenon of the emission of microwave radiation from InSb. Subsequently many experimental investigations were undertaken but no completely satisfactory explanation of the emission mechanism or mechanisms has been given.[2] Microwave radiation and rf current oscillations arise spontaneously whenever the applied current and applied magnetic field exceed certain threshold values. The emission of microwave radiation is classified according to the operating conditions for which it occurs. In high-purity InSb specimens, two regimes of radiation are observed: a low-field regime of radiation which occurs before the onset of bulk impact ionization ($E_0 \lesssim 150$ V/cm) and a high-field regime of more intense radiation which occurs after the onset of impact ionization ($E_0 \gtrsim 150$ V/cm). Particular attention has been given to the study of low-field microwave radiation because it is generated under conditions for which well-developed conduction carrier transport theories exist. Several theoretical models have been proposed to account for the low-field radiation, but only the acoustoelectric interaction model and a localized plasma-type interaction model have been definitely related to experimental results.[2]

In order to determine the fundamental origin of the low-field microwave radiation, a special experimental arrangement has been used in this investigation. Experimental results demonstrate that two distinct modes of low-field microwave radiation are present in InSb specimens. One mode of radiation, designated as the $B_{||}$ mode, prevails when the applied magnetic field is aligned parallel to the direction of current flow (along the long dimension) in an InSb specimen and the other mode of radiation, designated as the $B_{\perp}$ mode, prevails when the applied magnetic field is aligned transverse to the direction of current flow. These modes of radiation were discovered separately in earlier investigations.[3,4] The $B_{\perp}$ mode of radiation is strongly dependent upon the exact azimuthal orientation of the transverse magnetic field relative to the lateral faces of the InSb specimen. Azimuthal rotation of the InSb specimen relative to a transverse magnetic field results in a reproducible symmetrically anisotropic radiation pattern of twofold periodicity. Furthermore, the physical properties of the contacts of the InSb specimen are correlated with the spatial distribution of the $B_{\perp}$ mode radiation along the length of the InSb specimen and it is determined that the radiation is nucleated by localized high electric field regions in the vicinity of the contacts. A theoretical model, which incorporates a bulk acoustoelectric interaction of off-axis acoustic waves, has been formulated to help explain the $B_{\perp}$ mode of radiation. Computer analysis of the model predicts an azimuthal pattern of acoustic gain which is in good agreement with the azimuthal radiation patterns measured in this experiment and in other related experiments.[5–8]

Examination of the spatial distribution of the $B_{||}$ mode of radiation reveals that, in contrast to the $B_{\perp}$ mode, the $B_{||}$ mode of radiation is more uniformly distributed along the length of the InSb specimen. It is believed that the acoustoelectric interaction is also involved in the $B_{||}$ mode of radiation.

II. EXPERIMENTAL PROCEDURE

The basic experimental arrangement consists of a pulse circuit and a microwave radiation detection circuit. A pulser supplies high current values by means of low-duty-cycle voltage pulses which are applied across the InSb specimen in series with a 1-Ω current-viewing resistor. A rotatable electromagnet supplies magnetic fields up to 5 kG. The radiation detection circuit consists of a low-noise tunnel-diode amplifier followed by a superheterodyne receiver which is tuned to a fixed frequency of 10 GHz. The operating band-

FIG. 1. Typical instability characteristics showing the current pulse with attendant noisy rf current oscillations (upper trace: 1 A/div) and the detected microwave radiation (lower trace: arbitrary scale) as a function of time (horizontal scale: 1 μsec/div). In this figure $I_0+I_{rf}\simeq 1.8$ A$\pm$0.15 A, $P_\mu\simeq 30$ dB, $B_\perp=5$ kG and approximately 50 pulse cycles are recorded.

width of the radiation detection circuit is equal to the 10-MHz bandwidth of the i.f. amplifier stage and the measured single-sideband sensitivity of the detection circuit is -100 dBm. The microwave radiation power is measured in decibels above the detection circuit sensitivity level by determining the amount of attenuation added by a precision attenuator located in the X-band waveguide at the detection circuit input, which is required to reduce the time-averaged level of the radiation to the level of the detection circuit sensitivity. The presence of rf current oscillations is detected by direct viewing of the current pulse from an oscilloscope which has a 24-MHz bandwidth (Fig. 1).

A positionable cartridge assembly, which allows both rotational and translational positioning of the InSb specimen relative to the waveguide, has been used in this investigation (Fig. 2). The InSb specimen is mounted in the Teflon cartridge and the cartridge assembly is placed in an inductive post configuration in the X-band waveguide section which is directly immersed in liquid nitrogen (a remote-access sliding short terminates the specimen end of the waveguide section). By means of a simple system of gears which are remotely adjusted with long rods, the cartridge assembly can be moved either rotationally or translationally with respect to the waveguide. These movements are denoted, respectively, by the symbols X and ϕ in Fig. 2. The current pulse is supplied to the InSb specimen through ball-joint pressure contact terminals which are located on each end of the cartridge assembly. Rotation of the cartridge assembly determines the azimuthal ϕ orientation of the magnetic field whereas rotation of the electromagnet determines the polar θ orientation. Translational movement of the cartridge assembly relative to the radiation-gap assembly in the waveguide yields the spatial variation of the radiation along the length of the InSb specimen. The radiation-gap assembly consists of a pair of stainless-steel tubular shields which are inserted through opposite broad faces of the waveguide leaving a 1-mm gap in the center of the waveguide. Unless otherwise specified, all measurements reported here have been made with the radiation-gap assembly removed and the InSb specimen centered in the waveguide.

High-purity n-type InSb specimens which have typical dimensions of $10\times1\times1$ mm, with the long dimension oriented within 1° of a $\langle 110\rangle$ crystallographic direction, have been studied in this investigation. All measurements are made at a temperature of 77°K and under equilibrium low-field conditions near the end of the low-duty cycle 2–3-μsec current pulse (see Fig. 1). The radiation is observed at a fixed frequency of 10 GHz with the sliding short positioned for maximum radiation output at a point in the waveguide which is located from 3/2 to 5/2 wavelengths away from the radiating InSb specimen.

III. EXPERIMENTAL RESULTS

The physical properties of five n-type InSb specimens which have been studied in this investigation are listed in Table I. Microwave noise radiation is found in every InSb specimen except specimen D1. Although each of the radiating InSb specimens exhibit certain common radiation characteristics, discrepancies among the radiation characteristics are accounted for by the irregular nature of the specimen contacts. In agreement with George and Bekefi,[9] it has been found that specimens A1 and A2, which have tin contacts, exhibit the lowest radiation threshold fields of approximately 0.3 A ($\sim$25 V/cm) with $B_\perp=5$ kG. However specimen B1 which has In(Te) contacts, exhibits higher radiation threshold fields which exceed 1 A ($\sim$60 V/cm) with $B_\perp=5$ kG. Specimen A3 which has one In(Te) contact and one In contact will be described in detail in order to show how experimental discrepancies found in the radiation characteristics can be related to the physical properties of the contacts.

A. Dependence on the Orientation of the Magnetic Field

The positionable cartridge assembly used in this experiment allows simultaneous variation of both the

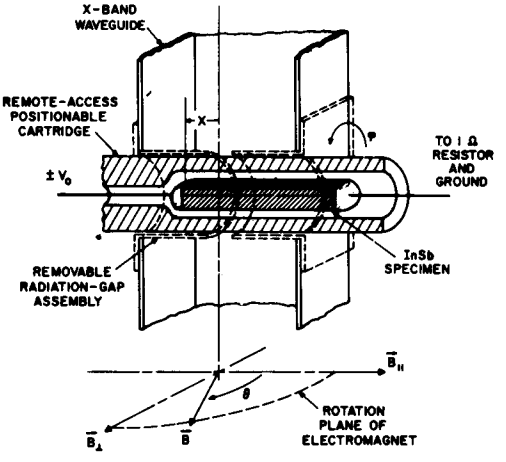

FIG. 2. Schematic drawing of positionable cartridge assembly (cross-sectional view).

TABLE I. InSb specimen properties at 77°K.

Specimen[a]	Dimensions (mm)	Conductivity [(Ω cm)$^{-1}$]	Hall mobility[b] (cm^2/V sec)	Carrier density (cm^{-3})	Ohmic resistance (Ω)	Composition of the contacts
A1	9.9×0.89×0.89	6.3	6.5×10^5	6.1×10^{13}	19.9	Sn
A2	7.4×0.79×0.79	7.6	6.5×10^5	7.3×10^{13}	15.6	Sn
A3	9.5×0.74×0.74	6.0	7.5×10^5	5.0×10^{13}	26.8	In/In(Te)[c]
B1	6.3×0.65×0.65	13.0	8.2×10^5	9.9×10^{13}	11.5	In(Te)
D1	9.2×0.87×0.87	245.0	9.7×10^4	1.6×10^{16}	0.45	In(Te)

[a] Specimens A1, A2, and A3 have been cut from a single slice of high-purity InSb. Specimen B1 has been cut from a different slice of high-purity InSb and specimen D1 has been cut from a Te-doped slice of InSb.

[b] The Hall mobility is determined from the asymptotic characteristic of a transverse magnetoresistance measurement.

[c] The contact connected to the ground side of the pulser is composed of In and the other contact is composed of In(Te) alloy (7% Te by weight).

azimuthal and the polar orientation of the applied magnetic field. Maintaining a constant applied current and a constant magnetic field strength, a typical low-field radiation pattern, as shown in Fig. 3, exhibits a strong dependence on the orientation of the magnetic field. The polar and azimuthal angles, θ and ϕ, are defined in Fig. 2. The zero reference of the azimuthal angles has been chosen so that the two prominent nulls of the $B_\perp$-mode azimuthal radiation pattern, $P_\mu(\phi)|_{\theta=\pi/2}$, occur near $\phi=\pi/2$ and $\phi=3\pi/2$. This choice of azimuthal reference angle permits direct comparison of the experimental results with the theoretical results (see Sec. V). The transverse component of magnetic field is directed out of a lateral surface of the InSb specimen (number A3) at $\phi=36°\pm10°$ and at all successive multiples of 90°.

As noted earlier there are two distinct modes of low-field microwave radiation. One mode of radiation, designated as the $B_\perp$ mode, prevails when the magnetic field is oriented transverse ($\theta=\pi/2$) to the direction of current flow in the InSb specimen and the other mode of radiation, designated as the $B_{||}$ mode, prevails when the magnetic field is aligned parallel ($\theta=0$ or π). As seen in Fig. 3, the $B_\perp$ mode of radiation exhibits an anisotropic azimuthal radiation pattern whereas the $B_{||}$ mode shows little dependence on the azimuthal angle. Although the average radiation level and exact structure of the radiation pattern depends on the polarity and strength of the applied fields, the general twofold-periodicity anisotropy characteristic of the $B_\perp$-mode azimuthal radiation pattern and the presence of a somewhat weaker isotropic $B_{||}$ mode is always observed. It was determined, in the following manner, that the radiation cannot be simply resolved into $B_\perp$ and $B_{||}$ components.

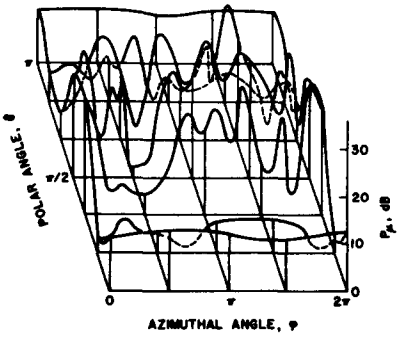

FIG. 3. Effect of the magnetic field orientation on the microwave radiation for specimen A3 when $|\mathbf{B}|=5$ kG and $I_0=-1.0$ A.

At the polar angles $\theta=\pi/6$ and $\theta=5\pi/6$, the transverse component of a 5-kG magnetic field is 2.5 kG and the parallel component is 4.3 kG. In an independent measurement it was found that if a purely transverse magnetic field is applied (maintaining $I_0=-1$ A at $\theta=\pi/2$), no detectable radiation is found for $B_\perp=2.5$ kG; whereas if a purely parallel magnetic field is applied (maintaining $I_0=-1$ A at $\theta=0$ or π), there is 12 dB of radiation at $B_{||}=4.3$ kG. The azimuthal radiation patterns at $\theta=\pi/6$ and $\theta=5\pi/6$ in Fig. 3 have an average radiation level of approximately 5 dB. Although the parallel component of magnetic field is equal to 4.3 kG at these polar angles, the radiation level is 7 dB less than the 12-dB radiation level which occurs when a purely parallel magnetic field of the same strength is present (maintaining $I_0=-1$ A in both cases). Furthermore the radiation patterns at $\theta=\pi/6$ and $\theta=5\pi/6$ retain some of the azimuthal anisotropy character of the $B_\perp$ mode of radiation even though a purely transverse magnetic field of the same strength cannot give rise to detectable radiation.

A resistance bridge was used to measure the low-field resistance ($I_0<10$ mA) and the polar magnetoresistance characteristic showed that the magnetoresistance monotonically increases, in direct proportion to the square of the transverse component of the magnetic field, as the magnetic field is rotated from a parallel to a transverse orientation. Weiss[10] has shown that this behavior indicates that the effects of inhomogeneities are not pronounced. Since the polar pattern of the radiation does not follow the polar

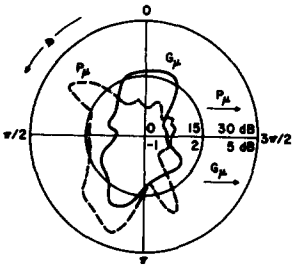

FIG. 4. Distortion of the azimuthal radiation characteristic at high radiation levels for specimen A3 when $B_\perp = 5$ kG and $\theta = \pi/2$. G_μ is the radiation threshold gain parameter normalized to $[(I_{0th})_\mu]_{max} = 1.2$ A and P_μ is the radiation power level measured at $I_0 = 1.4$ A.

magnetoresistance characteristic (the radiation intensity passes through a minimum in the neighborhood of 30° off the parallel alignment), it is concluded that the $B_{||}$ mode of radiation does not depend on the presence of inhomogeneities and that two distinct modes of radiation, the $B_\perp$ mode and the $B_{||}$ mode, exist in high-quality InSb.

Regardless of the physical nature of the contacts, the $B_\perp$ mode of radiation for each of the InSb specimens exhibits a reproducible anisotropic azimuthal radiation pattern of twofold periodicity. At high applied field values, much greater than the radiation threshold field values, the azimuthal radiation pattern sometimes develops into an asymmetrical shape. In order to delineate the low-level radiation characteristics, it is convenient to define a radiation threshold gain parameter $G_\mu \equiv P_\mu/(I_{0th})_\mu$, where $(I_{0th})_\mu$ is the applied current value which is required to generate a constant level of microwave radiation P_μ typically equal to 3 dB in excess of the detection circuit sensitivity level. Since the low-lying levels of microwave radiation always increase sharply with applied current, it is assumed that $(I_{0th})_\mu$ occurs before saturation effects set in and that G_μ is a measure of the radiation growth rate. Experimental data has been normalized to the minimum value of G_μ and plotted in units of decibels according to

$$G_\mu = 10 \log_{10}\{[(I_{0th})_\mu]_{max}/(I_{0th})_\mu\}.$$

For positive-polarity applied current, an asymmetrical azimuthal radiation pattern develops in specimen A3. Comparison of the azimuthal patterns of the radiation threshold gain G_μ and the resulting radiation power level P_μ at a high value of applied current, as shown in Fig. 4, reveals that the asymmetrical radiation pattern P_μ has developed whereas the threshold gain pattern G_μ is reasonably symmetrical. A premature saturation of the radiation develops at a power level of approximately 6 dB for $210° \lesssim \phi \lesssim 30°$. The important aspect of this measurement is that even though an asymmetrical azimuthal radiation pattern may occur, the fundamental radiation gain mechanism still exhibits a symmetrical azimuthal pattern of twofold periodicity.

The $B_{||}$ mode of radiation exists at applied current values which are far below the threshold of attendant $B_{||}$-mode current oscillations; however, it is found that either noisy or partially coherent spike-like current oscillations can occur in conjunction with the onset of the $B_\perp$ mode of radiation. Using a 3-GHz bandwidth sampling oscilloscope and a series of high- and low-pass filters, it has been established that the current oscillations consist entirely of submicrowave frequency (<1 GHz) components. A current oscillation threshold gain parameter G_{rf}, analogous to G_μ, is defined by using $(I_{0th})_{rf}$ in place of $(I_{0th})_\mu$, where $(I_{0th})_{rf}$ is the applied current value which is required to generate the first detectable evidence of current oscillations as viewed on an oscilloscope. In Fig. 5 it is seen that the azimuthal threshold characteristics of the 10-GHz radiation and the rf current oscillations have qualitatively similar patterns for both polarities of applied current. The general twofold periodicity of the $B_\perp$ mode of operation is present in all the characteristics. The joint similarity of the azimuthal patterns of G_μ and G_{rf} suggests that the microwave radiation and the rf current oscillations both arise from a common instability mechanism.

Using the resistance bridge, the azimuthal magnetoresistance pattern of specimen B1 was measured and is shown in Fig. 6. It reflects the square peripheral shape of the contacts and is not dependent on the polarity of the bridge current. The transverse magnetic field is aligned perpendicular to a lateral face of specimen B1 at $\phi = 40°$ and all successive multiples of 90°. These azimuthal orientations correspond to the maxima of the azimuthal magnetoresistance pattern (Fig. 6). The relative strengthening of the $\phi = 40°$ and $\phi = 220°$ peaks is due to a slight skew misalignment of specimen B1 in the positionable cartridge. Comparison of Figs. 5 and 6 shows that there may be a possible correlation between the azimuthal directions of maximum threshold gain and maximum magnetoresistance; however, the range of variation of the magnetoresistance pattern is only 8% (0.3 dB) whereas the range of variation of the threshold gain patterns falls between 1.4 and 3.6 dB (40% and 130%, respectively). If the azimuthal threshold gain patterns were simply a function of the geometry of the con-

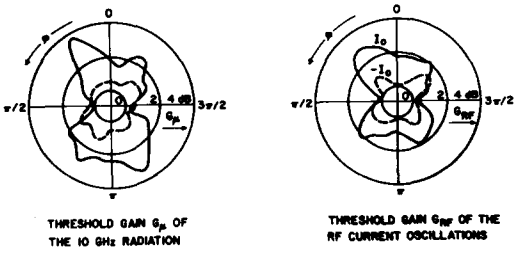

FIG. 5. Effect of current pulse polarity on the azimuthal characteristics of the instabilities for specimen B1 when $B_\perp = 5$ kG and $\theta = \pi/2$. Normalization current values for the G_μ curves: $[(I_{0th})_\mu]_{max} = 1.65$ A, -1.8 A and for the G_{rf} curves: $[(I_{0th})_{rf}]_{max} = 1.4$ A, -1.7 A.

tacts, the symmetrical fourfold periodicity of the magnetoresistance characteristic would be found in the azimuthal threshold gain patterns. Instead, the azimuthal threshold gain patterns exhibit a large symmetrical anisotropy of twofold periodicity which indicates that the anisotropy is not dependent upon geometrical effects. This conclusion is supported by independent measurements by Kokoschinegg and Seeger[11] who report that the azimuthal radiation patterns of circular cross-section InSb specimens also retain the anisotropy characteristic.

B. Evidence of Localized Radiation Nucleation Sources

With the radiation-gap assembly inserted in the waveguide, translational movement of the InSb specimen relative to the 1-mm radiation gap allows the measurement of the spatial distribution of the microwave radiation along the length of the specimen. Although the spatial resolution of this measurement is limited, it retains utility as a diagnostic tool.

A typical spatial distribution of the $B_\perp$ mode of radiation for positive-polarity applied current is illustrated by curve I of Fig. 7. Although the radiation is somewhat stronger at the anode end of the InSb specimen, maximum radiation is observed at a point which is approximately 6 mm from the cathode contact. However, when the transverse magnetic field is oriented near $\phi=305°$, an anomalously low threshold $B_\perp$ mode of radiation occurs which is shown in curve II of Fig. 7. It is found that the location of the maximum radiation peak is shifted 1.5-mm closer to the cathode contact. This behavior indicates that the anomalously low-threshold $B_\perp$ mode of radiation is enhanced by an interaction which occurs at the cathode end of the InSb specimen. Independent measurement of the transverse magnetoresistance characteristic of specimen A3 shows that a corresponding anomalous enhancement of the transverse magnetoresistance occurs at this azimuthal orientation of magnetic field. The magneto-

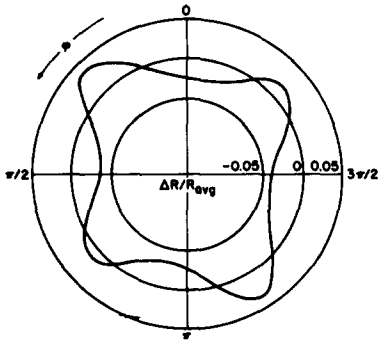

FIG. 6. Variation of the transverse magnetoresistance $\Delta R/R_{av}$ as a function of the azimuthal orientation of the transverse magnetic field for specimen B1 when $B_\perp=5$ kG, $\theta=\pi/2$ and $R_{av}=55.2\ \Omega$.

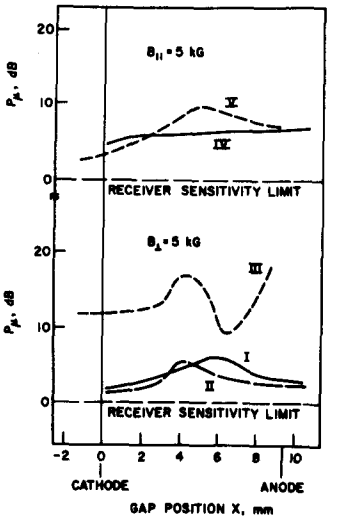

FIG. 7. Spatial distribution of the microwave radiation for specimen A3. (I) $I_0=1.4$ A, $\theta=\pi/2$, $\phi=15°$. (II) $I_0=0.4$ A, $\theta=\pi/2$, $\phi=305°$. (III) $I_0=-1.4$ A, $\theta=\pi/2$, $\phi=15°$. (IV) $I_0=1.4$ A, $\theta=0$, independent of ϕ. (V) $I_0=-1.4$ A, $\theta=0$, independent of ϕ.

resistance enhancement has been accounted for by the irregular peripheral shape of the In contact of specimen A3 wherein the contact extends into one corner of the specimen. Due to Hall field shorting effects at the In cathode contact, localized impact ionization exists at the edge of the contact.[12] It is believed that the anomalously low threshold $B_\perp$ mode of radiation in specimen A3 is nucleated by the presence of an unusually large impact ionization region at the extended edge of the In cathode contact.

If the operating conditions are changed to a typical case for which the radiation level is far above threshold, the maximum radiation level is found directly at the anode contact as shown in curve III of Fig. 7. Comparison of curves I and III shows that significantly greater radiation intensity results under negative-polarity applied current in specimen A3. For negative-polarity applied current, the In contact of specimen A3 serves as the anode contact. It has been shown[13] that In anode contacts inject holes into n-type InSb more readily than do In(Te) anode contacts. Curve III of Fig. 7 gives direct evidence of the nucleation of radiation by hole injection, localized at the anode contact. It is believed that the lack of direct evidence of the presence of hole injection at the anode contact in curve I of Fig. 7 may be due to the more Ohmic nature of the In(Te) contact which serves as the anode contact for positive-polarity applied current. A reasonably uniform spatial distribution of the $B_\perp$ mode of radiation has never been observed.

Curves IV and V of Fig. 7 show the spatial distribution of the $B_{||}$ mode of radiation. Under the operating conditions of curve IV, the more Ohmic In(Te) contact of specimen A3 serves as the anode contact and the radiation is uniformly distributed along the length of the specimen. However if the

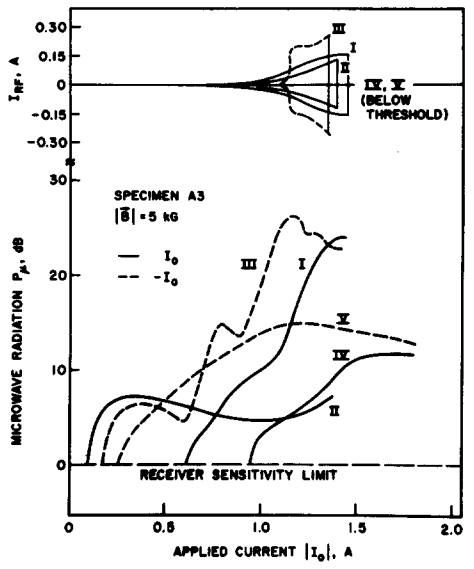

FIG. 8. Microwave radiation P_μ and rf current oscillation amplitude I_{rf} as a function of applied current for specimen A3. (I) $\theta=\pi/2$, $\phi=125°$. (II) $\theta=\pi/2$, $\phi=305°$. (III) $\theta=\pi/2$, $\phi=125°$. (IV) $\theta=0$, independent of ϕ. (V) $\theta=0$, independent of ϕ.

applied current polarity is reversed and the injecting In contact of specimen A3 serves as the anode contact, as shown in curve V, the radiation distribution becomes nonuniform and shifts toward the anode contact. This behavior is attributed to the existence of hole injection at the In anode contact which enhances the $B_{||}$ mode of radiation.

The radiation process is further clarified by the simultaneous study of the growth of the 10-GHz radiation and the rf current oscillations. In Fig. 8 curves I–III illustrate the growth characteristics of the $B_\perp$ mode of operation and curves IV and V illustrate the growth characteristics of the $B_{||}$ mode of operation. Curve I represents a typical growth characteristic of the $B_\perp$ mode of radiation, namely, a sharp onset of radiation which is followed by saturation effects which occur in conjunction with the gradual onset of noisy rf current oscillations. Curve II shows the anomalously low threshold growth characteristic of the $B_\perp$ mode of radiation which occurs only in the vicinity of $\phi=305°$ and only with positive-polarity applied current for specimen A3. As discussed previously, it has been shown that the anomalously low threshold $B_\perp$ mode of radiation is nucleated by localized impact ionization which is most pronounced for $\phi\simeq 305°$ because of the irregular peripheral shape of the In cathode contact. The anomalously low threshold radiation mechanism saturates at a radiation level of approximately 7 dB and supersedes the onset of a second radiation mechanism. The second radiation mechanism, evidenced in curve I of Fig. 8, is more common and occurs at higher applied currents. The study of its spatial distribution (as discussed in conjunction with curves I and III of Fig. 7) indicated that it is nucleated by hole injection which occurs at the anode contact.

A more complex anomalous-type growth characteristic, shown by curve III of Fig. 8, is found for negative-polarity applied current at an azimuthal orientation which is approximately 180° advanced from the azimuthal orientation of the positive-polarity anomalous-type characteristic of curve II. It is distinguished by three distinct radiation threshold levels occurring at −0.2, −0.6, and −0.9 A. The triple-resonance-type radiation growth characteristic of curve III is explained as follows. The sharp onset of radiation near threshold at −0.2 A is due to an impact ionization-type radiation nucleation source at the In(Te) cathode contact which generates the saturated radiation power level of 6 dB. The second radiation onset threshold which occurs at −0.6 A arises from a hole injection-type radiation nucleation source at the In anode contact. The radiation dip at the 15-dB power level which occurs at −0.9 A, corresponds to the threshold of noisy rf current oscillations. A sharp onset of large amplitude spike-like rf current oscillations occurring at −1.15 A corresponds to the final dip in the radiation power level. The latter two radiation power level dips are attributed to a redistribution of the spectral content of the energy of the interaction process from the microwave radiation frequency components into the rf current oscillation frequency components.

The growth characteristics of the $B_{||}$ mode of radiation, shown in curves IV and V of Fig. 8, are also characterized by a sharp onset of radiation which becomes saturated at a power level of approximately 15 dB. Since the threshold of the $B_{||}$-mode current oscillations occurs at values of applied current which are on the order of 2 A, the saturation of the $B_{||}$ mode of radiation at the lower applied current values shown in Fig. 8 is not related to the presence of current oscillations. The negative-polarity applied current threshold for radiation (−0.25 A), with the In contact serving as the anode contact, is significantly less than the positive-polarity threshold (0.95 A). Consideration of this result together with the study of the spatial distribution of the $B_{||}$ mode of radiation (curves IV and V of Fig. 7) substantiates the conclusion that hole injection at the In anode contact enhances the $B_{||}$ mode of radiation.

IV. PHYSICAL MODEL OF THE RADIATION PROCESS

The experimental results of Sec. III.A show that the symmetrical twofold periodicity characteristic of the azimuthal pattern of the $B_\perp$ mode of the radiation cannot be accounted for simply by the square cross-sectional geometry of the InSb specimen. Some

investigators[6,14] have attributed this anisotropy of the azimuthal radiation pattern to crystal inhomogeneities wherein a localized gain mechanism is enhanced along certain preferred directions. However, using the Weiss criterion,[10] magnetoresistance measurements in the present experiment have shown that the InSb specimens studied here possess no pronounced inhomogeneity effects. Furthermore, the reproducibility of qualitatively similar azimuthal radiation patterns in this experiment and in other related experiments,[5–8] suggests that this characteristic is not the result of random conditions.

Direct evidence of the existence of radiation nucleation sources, localized in the vicinity of the contacts, has been found in the present experiment (see Sec. III.B). Due to the high electron mobility in n-type InSb, the presence of a large transverse magnetic field gives rise to localized high-electric-field regions at diagonally opposite corners of the crystal.[12,15] As a result, localized impact ionization[12] or hole injection[13] may exist at the localized high-field regions and plasma-type streaming instabilities[16] may occur, but rapid recombination of the nonequilibrium holes would abruptly quench the interaction. Furthermore, it has been found in the present experiment that the maximum intensity of the low-field $B_\perp$ mode of radiation does not occur directly at the contacts, but rather is found near the center of the specimen. In an independent investigation of the acoustoelectric current oscillations in long InSb specimens, Seifert[17] found that, under conditions which are nearly identical to those of the present experiment, there is a statistical buildup of acoustic domains in the bulk of InSb specimens which are shorter than 14 mm. These observations indicate that the microwave radiation is dependent on the existence of acoustic disturbances.

There is considerable experimental evidence which shows that the low-field $B_\perp$ mode of microwave radiation is related to an acoustoelectric-type interaction.[5,7,18] In the presence of a large transverse magnetic field, the electron drift velocity at which maximum acoustoelectric gain occurs in n-type InSb is very low and is on the order of 5% of the electron thermal velocity. In the present experiment, this value of drift velocity corresponds to an applied current of approximately 0.2 A. If the physical mechanism of the radiation is a purely acoustoelectric interaction (as it is for long InSb specimens with length $\simeq$2 cm), maximum radiation should be observed near 0.2 A. However, in this experiment, radiation is observed at higher values of applied current. As discussed above, evidence has been obtained which indicates that the radiation mechanism is not a purely acoustoelectric interaction, but rather it depends on the presence of nucleation sources which exist in high-field regions which are localized in the vicinity of the contacts. Plasma-type streaming interactions[16] or simply shot

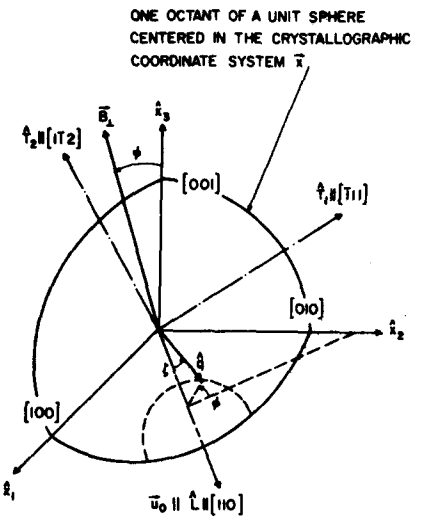

FIG. 9. Relative orientations of the transverse magnetic field $\mathbf{B}_\perp$, the acoustic wave $\hat{q}$ and the electron drift velocity $\mathbf{u}_0$. (The long dimension of the specimen is in the $\hat{L}$-direction and the transverse dimensions are in the $\hat{T}_1$ and $\hat{T}_2$ directions).

noise[15] may exist in these high-field regions, but it is assumed that these mechanisms only act as nucleation sources which excite, via piezoelectric forces, acoustic disturbances. In this way, large-amplitude acoustic disturbances are nucleated and emanate from the high-field edges of the contacts into the bulk of the specimen whereupon there is a statistical buildup of the disturbances.[17] As demonstrated by Arizumi *et al.*[19] the mere existence of the acoustic disturbances is not sufficient for the generation of microwave radiation since drifting electrons must be present in order to excite radiation from the collapsing acoustic disturbances. It is believed that the radiation mechanism is the electromechanical conversion[20] of acoustic energy into microwave radiation by means of the acoustoelectric interaction.[5,7,18] An acoustoelectric interaction is supported by electrons alone and will exist in the bulk of the InSb specimen where (in the present experiment) the low-field radiation is observed to originate. The radiation which arises at applied currents which exceed the 0.2-A value of maximum on-axis acoustoelectric gain is accounted for in two ways. First, higher applied currents are required to nucleate the large-amplitude acoustic disturbances and second; since the acoustic disturbances are excited in off-axis directions (due to Hall field-shorting effects at the contacts[12,15]), it is the off-axis acoustoelectric interaction which is involved in the radiation process and it can only achieve maximum gain for applied currents which are greater than 0.2 A. When all possible modes of off-axis acoustoelectric interaction are included, it is found (below) that the symmetrical twofold-periodicity characteristic of the azimuthal pat-

TABLE II. Physical parameters for n-type InSb at 77°K.

Parameter	Symbol	Value
Elastic constant	c_{11}	6.87×10^{10} N/m^2
Elastic constant	c_{12}	3.75×10^{10} N/m^2
Elastic constant	c_{44}	3.12×10^{10} N/m^2
Lattice mass density	ρ_m	5.77×10^3 kg/m^3
Piezoelectric constant	e_{14}	0.07 C/m^2
Dielectric constant	ϵ_{11}	$17.8\,\epsilon_0$
Electron effective mass	m^*	$0.013\,m_0$
Carrier concentration	N_0	1×10^{14} cm^{-3}
Thermal velocity	v_T	3×10^7 cm/sec
Carrier mobility	μ	6×10^5 cm^2/V sec
Specimen width[a]	w	0.1 cm

[a] Applied current is given by $I_0=Q_eN_0u_0w^2$, where Q_e is the electron charge and u_0 is the electron drift velocity.

tern of the $B_\perp$ mode of radiation is accounted for by a corresponding azimuthal variation of the resultant rms value of the off-axis acoustoelectric gain.

V. THEORY OF OFF-AXIS ACOUSTOELECTRIC INTERACTIONS

The growth rate of an acoustoelectric interaction is given by the product of an electromechanical coupling constant times a function of the macroscopic electronic and acoustic transport parameters. At the frequencies of interest, the electromechanical coupling constant arises primarily by means of piezoelectric coupling which is strongly dependent on the exact direction of acoustic-wave propagation relative to the lattice crystallographic orientation. In the crystallographic coordinate system $\mathbf{x}$ shown in Fig. 9, $\mathbf{B}_\perp$ is the applied magnetic field which is maintained transverse to the long dimension $\hat{L}$ of the InSb specimen (the direction of electron flow $\mathbf{u}_0$ is also parallel to $\hat{L}$); $\hat{q}$ is the direction of acoustic-wave propagation which is assumed to have been excited in the vicinity of the contacts; ζ is the inclination angle of the off-axis acoustic-wave propagation direction and ϕ is the azimuthal angle of the off-axis propagation direction. The same azimuthal angle ϕ also specifies the orientation of the transverse magnetic field $\mathbf{B}_\perp$ relative to the crystallographic axis $\hat{x}_3$ (because $\hat{q}$ is constrained to follow $\mathbf{B}_\perp$ through the Lorentz force which acts on the drifting electrons in the vicinity of the contacts where the acoustic waves are nucleated). Thus, as shown in Fig. 9, the inclination angle ζ is defined in the plane of the Lorentz force, namely, the $-\hat{q}\times\mathbf{B}_\perp$ plane which is tilted at the azimuthal angle ϕ.

Although a hydrodynamical theory of the acoustoelectric interaction is not strictly valid at frequencies as high as 10 GHz, it retains validity when sufficiently large transverse magnetic fields and low electron drift velocities are utilized. A theoretical analysis[21] has shown that the major correction required to extend Steele's theory[22] to higher frequencies is the inclusion of electron inertial terms. Steele's expression[22] for the acoustoelectric growth rate is modified in order to include the effects of electron inertial terms and it is written as

$$\alpha=-\kappa^2(\omega_R'/2v_s)\cdot[\gamma/(\gamma^2+W'^2)]\ \text{(rad/cm)}, \quad (1)$$

where κ^2 is the electromechanical coupling constant, v_s the acoustic wave phase velocity, $\gamma\equiv1-\mathbf{u}_0\cdot\hat{q}/v_s$, $W'\equiv(\omega_R'/\omega)+(\omega/\omega_D')$, ω the radian frequency of the acoustic wave, $\omega_R'=\omega_R/\nu_{\mathrm{Re}}'$ the effective dielectric relaxation frequency

$$\omega_D'=\frac{\omega_D\nu_{\mathrm{Re}}'}{(1-\gamma\nu_{\mathrm{Im}}'\omega_D/\omega)},$$

the effective diffusion frequency, ω_R the dielectric relaxation frequency, $\omega_D=\nu v_s^2/v_T^2$ the diffusion frequency at synchronism, ν the electron momentum-relaxation collision frequency, v_T the average thermal velocity of the electrons, $\nu_{\mathrm{Re}}'\equiv1+b'^2$, $\nu_{\mathrm{Im}}'\equiv\omega_\nu(1-b'^2)$, $b'^2\equiv b^2/(1+\omega_\nu^2)$, b the dimensionless $\mu B_\perp$-product, and $\omega_\nu\equiv\omega\gamma/\nu$ the parameter which includes the effect of electron inertial terms. When these inertial terms are neglected, $\omega_\nu\to0$, and (1) reduces to Steele's result.[22]

The off-axis acoustic-wave propagation conditions are determined by the solution of an eigenvalue matrix which gives three propagating waves; the longitudinal (compressional) acoustic wave and the fast- and slow-transverse (shear) acoustic waves. Corresponding to each of these waves, the off-axis electromechanical coupling constant $\kappa^2(\phi,\zeta)$ and phase velocity $v_s(\phi,\zeta)$ are computed using the following equations[23]:

$$\kappa^2=e_p^2/\epsilon_{11}c_\lambda, \qquad v_s=(c_\lambda/\rho_m)^{1/2}, \quad (2)$$

and

$$e_p=e_{14}[2(mn\xi_1+ln\xi_2+lm\xi_3)_\lambda/|\,\boldsymbol{\xi}_\lambda\,|], \quad (3)$$

where the subscript λ denotes that ξ_1, ξ_2, and ξ_3 are the components of the acoustic-wave eigenvector $\boldsymbol{\xi}_\lambda$ which corresponds to the effective lattice elastic constant eigenvalue c_λ; l, m, and n are the set of direction cosines measured in the crystallographic coordinate system $\mathbf{x}$ which correspond to ϕ and ζ (in Fig. 9); e_p is the effective piezoelectric constant; ρ_m the lattice mass density and ϵ_{11} and e_{14} are, respectively, the nonvanishing elements of the lattice dielectric tensor and piezoelectric tensor.

Using (2) and (3) to determine the appropriate values of $\kappa^2(\zeta,\phi)$ and $v_s(\zeta,\phi)$, these values are substituted into (1) to obtain the off-axis acoustoelectric growth rate of each of the three acoustic waves. Acoustoelectric gain is determined by the relation; $\text{Gain}=10\log_{10}[\exp(2\alpha)]=8.68\,\alpha$, dB/cm. The values

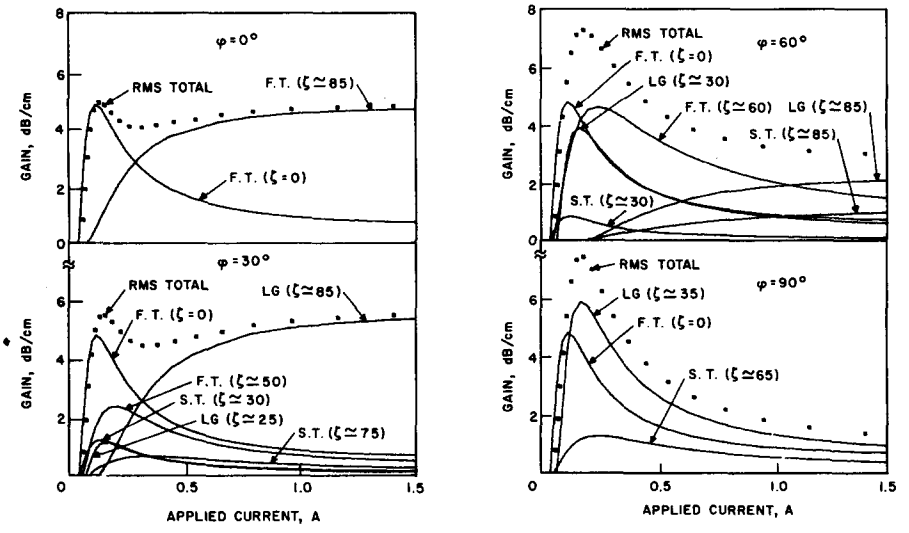

FIG. 10. Off-axis acoustoelectric gain in ⟨110⟩-oriented InSb at 10 GHz for $B_\perp = 5$ kG.

of the physical parameters which are suitable for n-type InSb at 77°K and which are used in this calculation are listed in Table II.

The off-axis acoustic wave propagates in the direction for which the acoustoelectric gain is maximum.[24] The results of this calculation are shown in Fig. 10 where only the maximum values of the acoustoelectric gain have been plotted. Off-axis gain has been computed for all three acoustic waves at selected values of the azimuthal angle ϕ [by symmetry, all possible values of the acoustoelectric gain are obtained in the range of azimuthal angles which is shown $(0 \leq \phi \leq 90°)$]. The longitudinal wave, the fast-transverse wave, and the slow-transverse wave are designated, respectively, as LG, F.T., and S.T. in Fig. 10 where the quantity in parentheses attached to the designation indicates the approximate inclination angle ζ at which the maximum off-axis gain is achieved. It is seen that, despite the stronger electromechanical coupling constant of the fast-transverse wave, the off-axis gain of the longitudinal wave can exceed the gain of the fast transverse wave. From (1) it can be shown that the enhancement of the gain of the longitudinal wave at 10 GHz is due to its relatively high effective diffusion frequency which allows more complete bunching of the drifting electrons. The resultant rms value of the off-axis gain, taking all possible acoustic waves into account, is also shown in Fig. 10. It is assumed that the intensity of the microwave noise radiation is proportional to the total rms value of the acoustoelectric gain. Radiation growth characteristics, at low applied currents, have been observed in the present experiment (see curves II and III of Fig. 8) which are similar to the shape of the rms gain characteristics in Fig. 10. However for applied currents above 0.5 A, the radiation intensity was observed to increase more rapidly than the rms gains of Fig. 10.

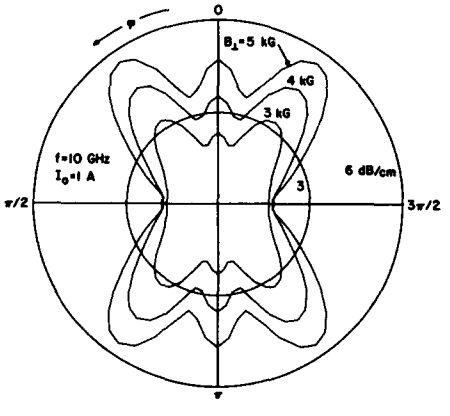

FIG. 11. Azimuthal pattern of the resultant rms value of the off-axis acoustoelectric gain in ⟨110⟩-oriented InSb at 10 GHz for $I_0 = 1$ A.

Direct comparison of the theoretical rms gain curves to experiments is difficult because of the variability of the nucleation conditions with applied current which are not described by this theory. This difficulty can be circumvented by maintaining the applied field strengths constant and examining the azimuthal dependence of the rms gain. The theoretical results are shown in Fig. 11. Comparison to the corresponding experimental results in Figs. 3–5 shows good correlation between the relative shape of the theoretical azimuthal patterns of rms acoustoelectric gain and the experimental azimuthal patterns of the $B_\perp$ mode of microwave noise radiation. The azimuthal variation of the off-axis rms acoustoelectric gain has also been calculated for conditions which are appropriate to other related experiments[5,7,8] and good agreement has been obtained.

VI. DISCUSSION AND CONCLUSIONS

Experimental results have indicated that, depending on the orientation of the applied magnetic field, there are two distinct modes of low-field microwave radiation in InSb, namely a $B_\perp$ mode and a $B_{||}$ mode. Although the radiation depends on localized nucleation mechanisms such as impact ionization or hole injection occurring in the vicinity of the contacts, the maximum intensity of the radiation is observed near the center of the InSb specimen. It is believed that acoustic disturbances are created by the localized nucleation mechanisms and the radiation arises from electromechanical conversion, via the acoustoelectric interaction, of off-axis acoustic disturbances into microwave radiation which occurs in the bulk of the InSb specimen.

A theory, incorporating the acoustoelectric interaction of off-axis acoustic waves, has been developed and the resultant azimuthal pattern of rms acoustoelectric gain accounts for the existence of the symmetrical twofold periodicity characteristic of the $B_\perp$ mode of microwave radiation from ⟨110⟩-oriented InSb. The appropriate azimuthal symmetries of the radiation characteristics which have been observed[6,7,11] in ⟨100⟩- and ⟨111⟩-oriented InSb are also explained by this theory. A much stronger off-axis acoustoelectric amplification of the acoustic disturbances will occur at lower frequencies and, because the specimens used in this experiment are not sufficiently long, noisy rf current oscillations will arise.[25] Thus the off-axis acoustoelectric gain mechanism, under different manifestations, can account for the joint similarity of the azimuthal patterns of threshold gain of the microwave radiation and the rf current oscillations which were observed in this experiment.

The results of the present experiment show the existence of a distinct $B_{||}$ mode of radiation, unrelated to the effects of inhomogeneities (as evidenced by magnetoresistance measurements), which is greatly diminished when the magnetic field is rotated 20°–30° away from the parallel orientation. Furthermore, the intensity of the $B_{||}$ mode of radiation is more uniformly distributed along the length of the specimen than it is for the $B_\perp$ mode of radiation. Recent experimental work by Gorelik *et al.*[26] has demonstrated that the presence of not only a transverse-, but also a parallel-magnetic field enhances the acoustoelectric interaction. It is believed that the $B_{||}$ mode of radiation observed here and the acoustoelectric enhancement of voltage observed by Gorelik *et al.*[26] arise from a common acoustoelectric mechanism which is dependent on the existence of a parallel magnetic field. No adequate theory for the $B_{||}$ mode of the acoustoelectric interaction has yet been developed.

ACKNOWLEDGMENTS

The authors wish to thank Professor W. Curtice for helpful discussions as well as W. Eaton, E. Kayser, and O. Wagner for their able technical assistance.

* This work was supported by the Air Force Systems Command's Rome Air Development Center.

[1] R. D. Larrabee, Bull. Amer. Phys. Soc. **9**, 258 (1964).
[2] M. Glicksman, IBM J. Res. Develop. **13**, 626 (1969).
[3] S. J. Buchsbaum, A. G. Chynoweth, and W. L. Feldmann, Appl. Phys. Lett. **6**, 67 (1965).
[4] D. K. Ferry, R. W. Young, and A. A. Dougal, Bull. Amer. Phys. Soc. **10**, 594 (1965).
[5] T. Arizumi, T. Aoki, and K. Hayakawa, J. Phys. Soc. Japan **25**, 1361 (1968).
[6] D. K. Ferry and W. A. Porter, IBM J. Res. Develop. **13**, 621 (1969).
[7] F. Seifert, L. Palmetshofer, and C. Schatzl, Electron. Lett. **5**, 288 (1969).
[8] J. Livingstone and W. Duncan, Brit. J. Appl. Phys. **2**, 1411 (1969).
[9] E. V. George and G. Bekefi, Appl. Phys. Lett. **15**, 33 (1969).
[10] H. Weiss, *Semiconductors and Semimetals, Physics of III–V Compounds*, edited by R. K. Willardson and A. C. Been (Academic, New York, 1966), Vol. I, pp. 315–378.
[11] P. Kokoschinegg and K. Seeger, Proc. IEEE **56**, 2191 (1968).
[12] A. H. Thompson and G. S. Kino, J. Appl. Phys. **41**, 3064 (1970).
[13] B. Ancker-Johnson and C. L. Dick, Jr., Appl. Phys. Lett. **15**, 141 (1969).
[14] C. W. Turner, IBM J. Res. Develop. **13**, 611 (1969).
[15] J. E. King, J. Appl. Phys. **40**, 5350 (1969).
[16] G. A. Swartz and B. B. Robinson, J. Appl. Phys. **40**, 4598 (1969).
[17] F. Seifert, Electron. Lett. **4**, 356 (1968).
[18] C. W. Turner, J. Appl. Phys. **39**, 4246 (1968).
[19] T. Arizumi, T. Aoki, and K. Hayakawa, J. Phys. Soc. Japan **26**, 370 (1969).
[20] H. E. Bommel and K. Dransfield, Phys. Rev. **117**, 1245 (1960).
[21] W. Fleming and J. E. Rowe, J. Appl. Phys. (to be published).
[22] M. C. Steele, RCA Rev. **28**, 58 (1967).
[23] C. S. Hartmann and A. Bers, Massachusetts Institute of Technology, Quart. Progr. Rep. No. 93, 139, 1969.
[24] A. R. Moore, R. W. Smith, and P. Worcester, IBM J. Res. Develop. **13**, 503 (1969).
[25] A. R. Moore, J. Appl. Phys. **38**, 2327 (1967).
[26] J. Gorelik, M. Zinman, B. Fisher, and A. Many, J. Appl. Phys. **41**, 445 (1970).